Visual Neuroscience (2004), **21**, 693–702. Printed in the USA.

DOI: 10.1017/S0952523804045043

Transmission of single photon signals through a binary synapse in the mammalian retina

AMY BERNTSON,[1] ROBERT G. SMITH,[2] AND W. ROWLAND TAYLOR[1,3]

[1]John Curtin School of Medical Research and Centre for Visual Sciences, Australian National University, Canberra, Australia
[2]Department of Neuroscience, University of Pennsylvania, Philadelphia, Pennsylvania
[3]Neurological Sciences Institute, Oregon Health & Sciences University, Beaverton, Oregon

(RECEIVED December 17, 2003; ACCEPTED June 2, 2004)

Abstract

At very low light levels the sensitivity of the visual system is determined by the efficiency with which single photons are captured, and the resulting signal transmitted from the rod photoreceptors through the retinal circuitry to the ganglion cells and on to the brain. Although the tiny electrical signals due to single photons have been observed in rod photoreceptors, little is known about how these signals are preserved during subsequent transmission to the optic nerve. We find that the synaptic currents elicited by single photons in mouse rod bipolar cells have a peak amplitude of 5–6 pA, and that about 20 rod photoreceptors converge upon each rod bipolar cell. The data indicates that the first synapse, between rod photoreceptors and rod bipolar cells, signals a binary event: the detection, or not, of a photon or photons in the connected rod photoreceptors. We present a simple model that demonstrates how a threshold nonlinearity during synaptic transfer allows transmission of the single photon signal, while rejecting the convergent neural noise from the 20 other rod photoreceptors feeding into this first synapse.

Keywords: Vision, Scotopic, Bipolar cell, Mouse retina, mGluR6, Electrophysiology

Introduction

Under scotopic conditions (starlight), visual sensitivity approaches the limit imposed by the availability of photons. Humans report the perception of light flashes resulting in the capture of less than ten photons in the retina (Hecht et al., 1942; Sakitt, 1972). Since signals from many hundreds or thousands of rod photoreceptors (rods) converge upon an individual optic nerve fiber, it is exceedingly unlikely that a single rod will capture all these photons. Therefore the single photon signal must be transmitted reliably through the successive synaptic relays within the retina. In cats, a single photon elicits 2–3 extra spikes in the optic nerve fiber connected to a retinal ganglion cell (Barlow et al., 1971; Mastronarde, 1983).

Mammals possess a specialized "rod pathway" within the retina which mediates vision under scotopic conditions (Famiglietti & Kolb, 1975; Dacheux & Raviola, 1986; Daw, et al., 1990). The rod pathway comprises a chain of three neural elements connecting the rods to the retinal ganglion cells. At the first synapse, the rods connect to a specialized second-order neuron, the rod bipolar cell (Dacheux & Raviola, 1986; Wässle, et al., 1991). The rod bipolar cells (RBCs) connect to a specialized rod amacrine cell, the AII amacrine cell (Strettoi et al., 1990; Chun, et al., 1993). Convergence within this rod pathway is highest across these first two synapses, from the rods to the RBCs and from the RBCs to the AII amacrine cells, resulting in a total convergence of more than 1000 rod signals to a ganglion cell (Sterling et al., 1988; Strettoi et al., 1990; Tsukamoto et al., 2001). Such a large convergence allows many single photon signals to be summed by higher-order neurons. Since each rod receives one photon or less per integration time (~0.2 s) at scotopic background levels, the signal convergence within this circuit can account for much of the dynamic range of the interneurons under scotopic conditions, which therefore implies spatio-temporal integration over the entire scotopic range.

Convergence also pools the background neural noise, and it has long been recognized that without some mechanism to suppress noise, the sparse single photon signals would become swamped by the convergent noise (Baylor et al., 1984). One likely mechanism for removing this noise is a nonlinear threshold at the synapse between rods and the RBC (van Rossum & Smith, 1998; Field & Rieke, 2002). This present study had two goals: to resolve the amplitude and time course of the single photon signal in the RBCs, and to examine possible mechanisms of noise suppression at the rod to RBC synapse.

Materials and methods

Preparation and recording

The methods used have been described previously (Berntson & Taylor, 2000). All experimental manipulations involving animals were approved by the Animal Experimentation Ethics Committee

Address correspondence and reprint requests to: W. Rowland Taylor, Neurological Sciences Institute, Oregon Health & Science University—West Campus, 505 NW 185th Avenue, Beaverton, OR 97006, USA. E-mail: taylorw@ohsu.edu

of the Australian National University. The animals were killed with a lethal intraperitoneal injection of Nembutal (0.1 ml, 100 mg/ml) and the eyes immediately enucleated and placed in oxygenated Ames' medium at room temperature. Retinas were isolated from dark-adapted Black6 mice, 4–6 weeks of age. Vertical slices of retina, about 200–400 μm thick were prepared under infrared (>850 nm) illumination, and maintained in a recording chamber, which was continuously perfused at a rate of 3 ml/min with oxygenated Ames medium (Sigma Chemical Co., St. Louis, MO). The temperature was controlled at 35°C. Intracellular solutions were aliquoted and stored at −20°C until ready for use, and contained (in mM) 110 Cs-Gluconate, 5 NaCl, 0.1 $MgCl_2$, 0.1 EGTA, 5 Na-HEPES, 5 ATP, and 5 GTP. The pH was adjusted with CsOH to 7.4. Na-ATP and Na-GTP were prepared as 100 mM stock solutions in water, stored at −20°C, and added to the intracellular solution on the day of the experiment. In some experiments, 0.05% Lucifer yellow was included in the intracellular solution, and epifluorescence microscopy used to visualize the morphology of the cell at the conclusion of the recordings. Whole-cell patch-clamp recordings of membrane currents were made from visually identified rod bipolar cells using an EPC-9 patch amplifier (HEKA Electronik, Lambrecht, Germany). The holding potential was set to −50 mV. Currents were filtered through a 4-pole Bessel filter at a half-power frequency of 2 kHz, and sampled at 5 kHz. Further digital filtering was performed during subsequent data analysis. Errors are quoted as standard deviations.

Rod bipolar cells were initially targeted as having an inverted pear-shaped soma located adjacent to the outer plexiform layer, with a single axon projecting straight down towards the inner plexiform layer. In early experiments, the identity was confirmed by visual inspection of the Lucifer yellow filled cells at the conclusion of the experiment. Subsequently, we relied upon the observable anatomical features, the characteristic form of the light responses, and the absolute light sensitivity. The anatomical features obviated the possibility that we were recording from either amacrine or horizontal cells. The sensitivity and form of the light responses distinguished between rod and cone bipolar cells.

Light stimuli

Full-field light stimuli generated on a Macintosh computer monitor were imaged onto the preparation through the 40×/0.8NA microscope objective. Neutral density filters were placed in the light path to attenuate the light by 2 log units. Only the green phosphor of the computer monitor was used for the stimulus. The light intensity emitted by the green phosphor was measured at 10-nm intervals over the visible range, and was characterized by a single monotonic peak at 540 nm with a width at half the peak height of 75 nm. Light delivered to the rods through the microscope objective was measured at the preparation plane in lumens/m^2 using a calibrated photometer (United Detector Technology, Hawthorne, CA). The stimulus intensity was then converted to a power density (W/m^2), assuming 683 lm/W (Wyszecki & Stiles, 1967). Accounting for the spectral emission of the green phosphor, and the photometric filter transmission produced a corrected conversion factor of 683 × 0.82 = 560 lm/W. The emission spectrum of the green phosphor was then converted to photons/m^2. The photon density available to stimulate the rods was determined from the overlap (multiplication) of the rhodopsin sensitivity spectrum (Lamb, 1995), and the emission spectrum of the green phosphor. Light stimuli are quoted as the equivalent flux of 500-nm wavelength photons. Unless otherwise noted, a flash stimulus comprised a single frame, nominally of 13.3-ms duration (monitor refresh rate 75 Hz), and therefore intensity is given simply as photons$\cdot\mu m^{-2}\cdot$flash^{-1}. The half-maximal saturation point in Fig. 1 was calculated to be about 1.3 photons$\cdot\mu m^{-2}\cdot$flash^{-1}. Since only a small region of the monitor screen was imaged onto a rod outer segment, the actual duration of the light flash at an outer segment was ~2 ms, with an exponential decay of less than 1 ms. The stimulus monitor intensity was approximately linearized using a look-up table. Residual errors were obviated by measuring the intensity of each stimulus over the same screen area imaged onto the preparation. We did not directly measure the spontaneous rate of single photon events, which could have been higher than encountered *in vivo* due to stray light, including photons emitted from the "black" monitor screen.

Analysis of variance

A full protocol consisted of a series of 30 trials delivered at a rate of 2 Hz at each of four intensities. A trial comprised a single frame flash. The response amplitude in each trial was measured by matched filtering, a method that efficiently extracts the amplitude of events with known waveform from a noisy signal. Our implementation was essentially as described previously (Baylor et al., 1979; Ashmore & Falk, 1980). All responses within the linear range were averaged together, and this normalized response was used as the filter impulse response, or template, for the single photon event. These filter templates were used to calculate the shape factor referred to in the text. At each intensity the amplitudes of each of the 30 flash responses, a_i, were estimated according to the equation:

$$a_i = k\int \bar{R}(t)r_i(t)\,dt, \qquad i = 1,2\ldots30,$$

where $\bar{R}(t)$, is the normalized filter template with peak amplitude of 1, $r_i(t)$ is the ith response, and the scaling factor $k = 1/\int \bar{R}(t)^2\,dt$. If the variance in the response amplitudes was dominated by random photon capture in the connected rods, then the single photon event amplitude can be calculated from the ratio of the slopes of the initial linear portions of the intensity–response relations shown in Figs. 3A and 3B. Thus, this estimate of the single photon event amplitude, i_q, is independent of the particular model used to account for the saturation in the variance observed at higher stimulus intensities.

All of the data were fit to the relevant equations using the Levenberg-Marquardt nonlinear least-squares algorithm as implemented by the Igor analysis package (WaveMetrics, Lake Oswego, OR).

Models of synaptic transmission

Two models were constructed to account for the saturation of the variance of the RBC responses—the Poisson model and the Transmission model. Both models have a rod bipolar cell receiving input from N_r identical rods. Each rod sums photons linearly, and makes a single, synaptic connection with the RBC. The signal detected by the recording electrode represents the aggregate current from all of the rod inputs. A critical feature of the models is a limitation on the number, q, of single photon events that can be transmitted through

each synapse. This property is handled differently in the two models.

In the Poisson model, synaptic transmission between a rod and a RBC is assumed to saturate when the number of photons captured by a rod is $\geq q$. If $q = 1$, then the postsynaptic response saturates whether one, two, or more photons are captured by the rod. Such a synapse signals the occurrence or not of a photon or photons, and we call this a binary synapse. If the probability that photons are captured and transmitted by the rods is Poisson distributed, then the mean current in the rod bipolar cell is given by,

$$\bar{I}_m = I_{\max}(1 - e^{-L\phi}), \tag{1}$$

where I_{max} is the saturating response amplitude in amperes, L is the flash intensity in photons$\cdot\mu$m^{-2}, and ϕ is a light-intensity constant with units of μm^2/photon. The range over which the bipolar cell current saturates is determined by the effective photosensitivity of the connected rods. Therefore the light-intensity constant, ϕ, represents the effective collecting area of the rods in the slice preparation, and the mean photon capture rate, $L\phi$, is equivalent to photoisomerizations per rod (Rh*/rod). In Figs. 1, 3, and 4 we have converted flash intensities to equivalent Rh*/rod, using the collecting area derived from the fit of eqn. (1) to the data in Fig. 1B.

The variance in the mean response amplitude for the binary synapse is given by,

$$\sigma^2 = I_{\max} i_q (1 - e^{-L\phi})(e^{-L\phi}), \tag{2}$$

where i_q is the single photon signal amplitude. For small L, $e^{-L\phi} \rightarrow 1$, and rearranging eqns. (1) and (2) produces

$$\sigma^2 = I_m i_q. \tag{3}$$

We can determine i_q from eqn. (3), by plotting the variance against the mean current, and finding the slope of the line. Since each rod could contribute at most a single photon signal to the bipolar cell, we can use i_q and the saturating current $I_{\max}$, to obtain an estimate for the number of rods converging onto a bipolar cell as $N_r = I_{\max}/i_q$. These estimates from physiological methods compared very favorably with estimates derived from anatomical reconstructions.

The Transmission model is used to examine the effects of a threshold on noise suppression at the synapse. For this purpose, the parameter values were chosen such that a single photon in the rod produced a saturating postsynaptic response, that is. the synapse is binary. A photon in a rod reduced the normalized glutamate concentration in the synaptic cleft according to the equation:

$$glut = 1 - \frac{ph^{ha}}{k_a^{ha} + ph^{ha}}, \tag{4}$$

where $0 \leq glut \leq 1$, ph is a Poisson distributed random variable describing the number of photons captured by the rod, k_a determines how many photons are required to half-saturate the presynaptic output, and ha determines the cooperativity of the process. In noise-free simulations, ph took integral values including zero. The S/N ratio of the single photon response in the rod could be simulated by adding to ph a value randomly selected from a Gaussian distribution. Two Gaussian distributions were used; a baseline noise distribution with standard deviation σ_d when $ph = 0$, and a single photon event amplitude distribution with standard deviation σ_q when $ph > 0$ (Fig. 4). Glutamate activates the postsynaptic mGluR6 receptors according to the equation:

$$mG = \frac{glut^{hb}}{k_b^{hb} + glut^{hb}}, \tag{5}$$

where mG represents the activated receptor and k_b and hb are the binding affinity and cooperativity, respectively. Receptor activation modulates a postsynaptic biochemical cascade, which ultimately reduces the open probability, p, of postsynaptic cationic channels. For simplicity, we assume that the biochemical cascade is not saturated when $mG \rightarrow 1$, and thus can be modeled according to the equation:

$$p = 1 - B \times mG, \tag{6}$$

where $0 \leq p \leq 1$ and B is a biochemical gain factor similar to that described by Shiells and Falk (1994). The resulting current in the RBC is given by

$$I_{\mathrm{RBC}} = \sum_{i=0}^{N_r} p_i i_q, \tag{7}$$

where p_i is the open probability from the ith rod, i_q is the single photon amplitude, and N_r is the number of rods. The response of the bipolar cell was obtained by averaging 5000 trials at each intensity. For each trial, the value for ph [eqn. (4)] in each of the N_r rods connected to the RBC was drawn from a Poisson distribution. When testing the effects of noise on the system, the amplitude of these events, as a fraction of the single photon event amplitude, was made variable by the addition of Gaussian-distributed noise as described above. The resulting current was added to the response of the RBC [eqn. (7)]. The variance was calculated from the trial-to-trial difference from the mean response.

Results

The flash intensity–response relation was determined for dark-adapted rod bipolar cells in order to establish the intensity range appropriate for the adaptation level of the preparation. Flashes, comprising a single video frame, elicited transient inward currents in the RBCs (Figs. 1A & 1B solid symbols, 13 cells). The open symbols in Fig. 1B were obtained in a separate series of experiments in which the responses to 30 consecutive flashes were averaged (7 cells). We found that the amplitude of the peak flash-evoked currents as a function of flash intensity was described by a saturating exponential [eqn. (1), solid line Fig. 1B] over the entire intensity range tested. At low flash strengths, the limiting slope of the intensity–response relation on the log–log plot was unity, consistent with the expectation that doubling the intensity should double the mean number of photons captured and thus produce a proportionate increase in the mean current amplitude. Linear scaling of responses at low intensity is also shown in Fig. 2C. Intensity–response relations in mouse rod bipolar cells have also been described by the equation,

$$I_p = I_{\max} L^h/(L^h + L_{1/2}^h), \tag{8}$$

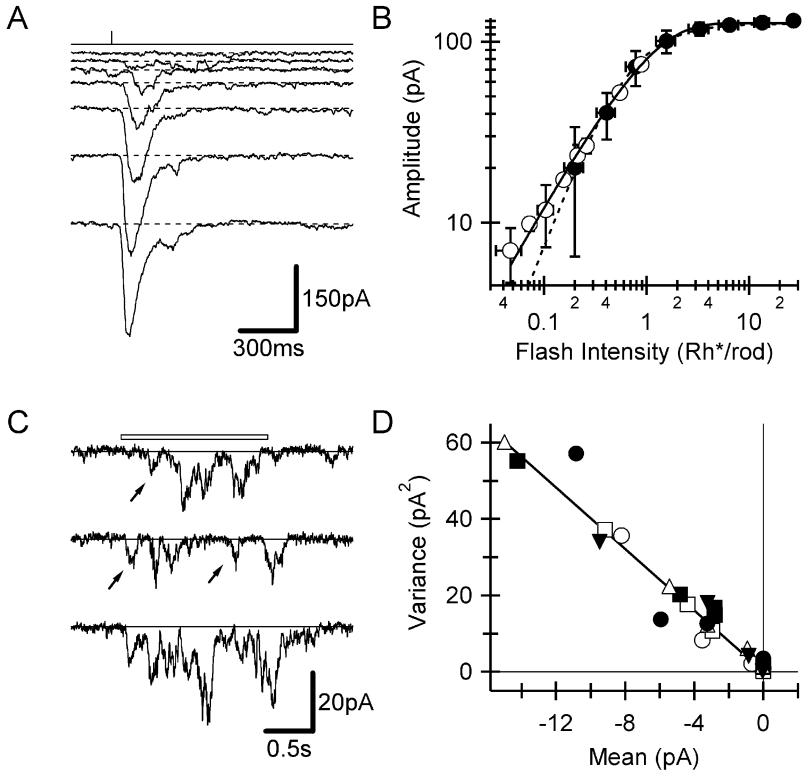

Fig. 1. Estimation of the single photon amplitude from analysis of the variance. A: Responses to single flashes of increasing intensity in one cell. The vertical mark at the top marks the flash time. Flash intensities were 0.1, 0.2, 0.5, 0.9, 1.4, 2.6, and 4.3 Rh^*/rod. B: Absolute amplitude of flash responses. The peak flash response is plotted against stimulus intensity. In the individual cells, the amplitude at each intensity was measured either from single flashes (solid symbols, 13 cells), or as the average of 30 flashes (open symbols, 6 cells). The responses in each cell have been normalized by a factor equating the saturating amplitude to the average for the group of cells. Similarly, intensity values have been normalized by a factor equating the half-maximal intensity with the mean for the group of cells. Each point represents the average of responses obtained over a small range of intensities. Error bars for the amplitudes and intensities are standard deviations. The solid line shows the prediction from eqn. (1), with $I_{max} = 126$ pA and $\phi = 0.54\ \mu m^2$/photon. The dotted line shows the best fit of eqn. (8) to the solid data points, with $L_{1/2} = 0.63$ Rh^*/rod and $h = 1.54$. C: Current responses in a RBC elicited by a long light step. The arrows highlight possible single-photon events. Light intensities were 0.06, 0.20, 0.60 Rh^*/rod/sec. D. Variance versus mean for 5 cells from records similar to those shown in *C*. The fitted line has a slope = −4.02 pA, corresponding to a single-photon amplitude of −5.95 pA (see Results).

where I_p is the peak current, L is the flash intensity, I_{max} is the amplitude at saturation, $L_{1/2}$ is the half-saturating flash intensity, and h is the Hill coefficient (Field & Rieke, 2002). The parameters for the best fit were $I_{max} = -132 \pm 2$ pA, $L_{1/2} = 0.63 \pm 0.02$ Rh^*/rod, and $h = 1.54 \pm 0.05$ (Fig. 1B, dotted line). While this equation fitted well at high intensities, it deviated significantly at low intensities as it predicted a limiting slope equal to h. To examine the mechanisms of single photon signal transfer in more detail, we decided to obtain an estimate of the single photon signal amplitude.

Two protocols were employed to estimate the amplitude of the single photon signal in rod bipolar cells, both yielding similar results. An initial estimate was derived from analysis of the current variance elicited by long light steps (Fig. 1C). The arrows point to events displaying the amplitude expected for single photon signals (~5–6 pA). At higher intensities, numerous events appear to have superimposed to produce a response with variance much higher than the baseline variance. In five cells, the variance measured during the light step is plotted against the mean current measured during the same time period (Fig. 1D). At these low intensities, the variance–mean plot was approximately linear, and for each cell, the amplitude of the single photon signal, i_q, was calculated as $i_q = s\sigma^2/\bar{I}_m$ (Ashmore & Falk, 1982), where σ^2 is the variance, $\bar{I}_m$ is the mean current, and s is the average shape factor. The shape factor was calculated by numerical integration of the single photon signal waveform (see below) to be 1.51 ± 0.06 ($n = 7$). This yielded a single photon signal amplitude of 5.95 ± 1.7 pA ($n = 5$). While these results provided an indication of the single photon amplitude, they did not reveal the time course of the events. To verify our estimate of the single photon event amplitude, and to extract the time course of the single photon events, we analyzed RBC responses to brief flashes of dim light.

Flash stimuli, comprising a single video frame, were repeated at a rate of 2 Hz until 30 records had been captured at each of three or four light intensities. The results presented here were obtained from seven cells in which the recordings were stable enough to complete the full experimental protocol. Single responses to the lowest stimulus intensity were highly variable (Fig. 2A); however, averaging together all responses at a given intensity revealed the time course of the underlying signal (Fig. 2B). As a control, the intermediate stimulus intensity was presented during the first and last 30 stimuli. The close agreement in the amplitudes at the beginning and the ending of the recording period indicates that neither run-down nor adaptation significantly affected the responses. A smooth curve is fitted to each averaged response over the first 240 ms, according to the equation, $I = I_{max}[(t/\tau)\exp(-t/\tau)]^{n-1}$. This equation has been used to provide an empirical description of the flash response in mammalian rods, and describes the impulse response of an n-stage Poisson filter, with time constant, τ. In monkey and rat rods, $\tau \sim 200$ ms, and $n \sim 4–6$ (Penn & Hagins, 1972; Baylor et al., 1984). Recent measurements from mouse rods indicate that the time-to-peak of the single photon response is ~130 ms (Hetling & Pepperberg, 1999; Calvert, et al., 2000, 2001), which is very similar to our observations in mouse RBCs which displayed $\tau = 135 \pm 18$ ms and $n = 8 \pm 1$. The fitted curve in Fig. 2B declined more rapidly than the response, for $t >$ ~240 ms. This was a common feature, and mirrors a similar phenomenon in the single photon responses of monkey rods (Baylor et al., 1984). In the next section, we analyze the variance of the flash responses, on the assumption that they arise from superposition of identical single photon signals. Superposition of the underlying signals appears to be linear at low intensities, as is evident from a comparison of responses normalized to the flash intensity (Fig. 2C). In five neurons, the ratio of the normalized amplitudes

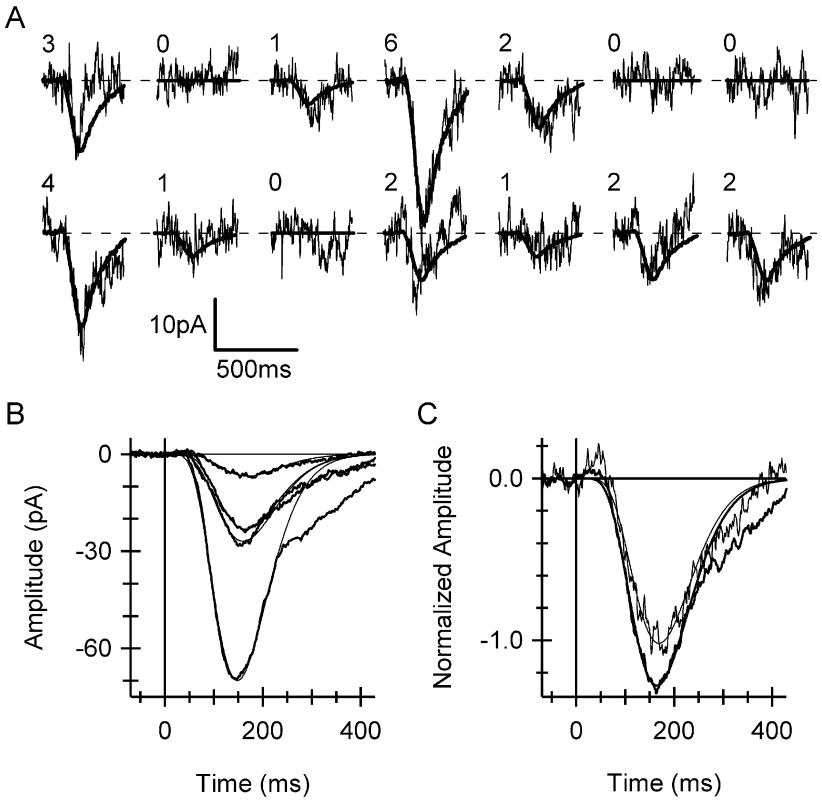

Fig. 2. Flash responses from a mouse rod bipolar cell. A: Representative responses to single flashes at about 0.09 Rh^*/rod, which for a convergence of ~20 rods produces ~1.8 Rh^*/flash in the RBC. The superimposed lines show the template for the matched filter, with an amplitude equal to the single photon event amplitude multiplied by the number above the record. B: Average responses each to a series of 30 light flashes delivered at 2 Hz. Flash intensities delivered about 0.09, 0.24, and 0.9 Rh^*/rod. To control for run-down of the response, the lowest and highest intensity stimuli were bracketed by two repetitions of the intermediate intensity. The amplitudes of the two middle traces were very similar indicating that run-down was not significant. The solid lines represent the best fit of an 8-stage Poisson filter (τ = 160 ms) over the first 240 ms. C: The amplitudes of the responses to the lowest and intermediate flash intensities have been normalized to the flash intensity. The similar amplitudes are consistent with linear summation of single photon events at low flash strengths.

at low intensities and intermediate intensities was 1.1 ± 0.2. The intensities differed by a factor of 3.

It was not possible to pick single photon signals from individual records with assurance. This was a limitation of the recording configuration, as it was difficult to maintain stable, low-noise recordings from these small cells for long periods. Nonetheless, the waveform of the underlying signals could be readily discerned from averaged records (Fig. 2B). We used this waveform as a matched-filter template (see Methods) to estimate the amplitude of the single photon signal that would reproduce the mean and variance observed for the data set. At low light intensities, the mean and variance of the filter estimates increased approximately linearly with light intensity (Figs. 3A & 3B), as was observed for the long light steps (Fig. 1D). The ratio of the initial slopes in Figs. 3A and 3B (shown by the straight lines) yielded a single photon amplitude of 5.5 pA.

The data in Fig. 3 shows that as the light intensity increases the variance of the responses appears to saturate earlier than the mean response. A model that incorporates basic elements of the synaptic arrangement can explain this observation (see Methods for details of the model). Anatomical reconstructions from electron micrographs indicate that a single RBC in mouse retina receives input from ~22 rods (Tsukamoto et al., 2001). At scotopic backgrounds, when the rods receive only one or zero photons per integration time, the rods act as linear photon counters (Baylor et al., 1984). Our data shows that at low intensities the RBC sums the synaptic inputs linearly. The critical feature of the model, which accounts for the saturation in the observed variance, is the proposal that a single photon signal saturates the synapse (Rao-Mirotznik, et al., 1995; van Rossum & Smith, 1998). Using the single photon signal amplitude, i_q = 5.6 pA (Table 1), the measured variance as a function of light intensity predicted from eqn. (2) is in good agreement with the data over the full intensity range tested (solid line, Fig. 3A).

Because the maximum signal that each rod can contribute is equal to the single photon signal amplitude, the maximum current in the rod bipolar cell is equal to the single photon signal amplitude multiplied by the number of convergent rods (N_r). Since I_{max} was measured from a saturating flash in each cell, we could estimate N_r as the ratio I_{max}/i_q. Although N_r was variable amongst the RBCs in the sample, on average N_r = 23 ± 8 (see

Table 1. *Summary of the variance-mean analysis*[a]

Cell	I_{max} (pA)	i_q (pA)	N_r
1a	−75	−5.48	14
2a	−94	−7.19	13
3a	−114	−4.24	27
4a	−170	−7.81	22
5a	−144	−3.61	40
6a	−103	−4.26	24
7a	−180	−6.22	29
1b	−110	−6.1	18
2b	−110	−7.7	14
3b	−87.6	−5.5	16
4b	−94.1	−3.3	29
5b	−173	−7.1	25
Mean	−121	−5.6	23
σ	36	1.2	8

[a]Matched filter analysis was performed on cells with the 'a' suffix, while the variance–mean analysis was applied to the 'b' cells. Both sets of results have been pooled in the average and standard deviations.

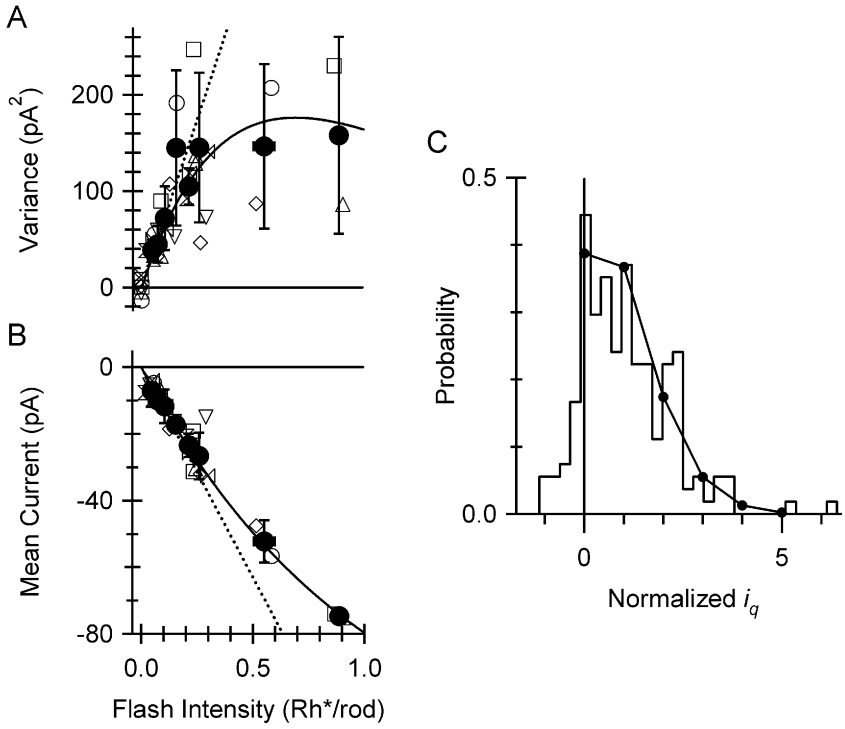

Fig. 3. Estimation of the single photon event amplitude. The variance (*A*) and mean (*B*) of the responses, calculated as described in the Methods, are plotted against the stimulus intensity (open data points). The amplitudes in each cell have been normalized by a factor equating the saturating amplitude to the average for the group of cells. The variance was scaled by the square of the factor. Intensity values have been normalized by a factor equating the half-maximal intensity with the mean for the group of cells. The black symbols show the average of the open symbols, each over a small range of intensities. Error bars are standard deviations. The dotted lines show the expectation for a linear increase in the variance and mean, with a single photon amplitude of −5.6 pA (see Table 1). The solid line shows the predictions for the Binary Poisson model, generated using the average values of i_q = 5.6 pA, I_{max} = 126 pA and ϕ = 0.54 μm^2/photon for the group of cells. In each cell, the average baseline variance recorded in the absence of stimulation has been subtracted from the variance measurements. C: Amplitude histogram of 210 responses in seven cells at the lowest intensity in each cell. The average stimulus intensity was ~0.05 Rh*/rod (lowest open symbol in Fig. 1B). The solid symbols show the prediction from a Poisson relation, assuming a convergence of 22 rods onto the RBC.

Table 1), in very good agreement with the anatomical convergence of rods onto RBCs observed in mouse retina (Tsukamoto et al., 2001). The convergence of rods onto the RBCs can also be estimated from the slope of the line in Fig. 3B if the single photon signal amplitude is known. Using the single photon amplitude above, the convergence is calculated to be ~21 rods onto each rod bipolar. This calculated number of convergent rods was consistent with the amplitude distribution of the responses. We used i_q to normalize the individual response amplitudes from all the cells at the lowest intensity, and generated a probability distribution for the flash response amplitudes in the RBC (Fig. 3C). The histogram was constructed from 210 responses in seven cells. The mean intensity for the group was ~0.05 Rh*/rod. As expected the distribution is skewed, with peaks corresponding approximately to integral multiples of i_q. The solid points above the histogram show the Poisson prediction for a mean capture rate = 22 rods × 0.05 Rh*/rod ~ 1 Rh*/RBC/stimulus.

The results suggest that each rod to RBC synapse is binary, signaling detection of a photon by the rod, and that these signals are summed linearly at the RBC soma. While the binary Poisson model is accurate, it does not give much insight into synaptic mechanisms. Moreover, it assumes that synaptic transmission is noise free. To investigate the effects of neural noise on synaptic transmission, we developed an alternative model that would break the transmission into smaller steps, more amenable to simulation and analysis.

The Transmission model is described in the Methods, and in addition to ϕ, i_q, and N_r, it included five additional parameters. Two describe the release of glutamate from the rod photoreceptors [eqn. (4)]. Two more describe binding and cooperativity for activation of the postsynaptic mGluR6 receptors [eqn. (5)]. A fifth represents the biochemical gain that links mGluR6 receptor activation with modulation of the postsynaptic channels [eqn. (6)]. The prediction from a noise-free simulation using this model, with B = 1.05, ha = 2, and hb = 4, k_a, k_b = 0.5, was indistinguishable from the binary Poisson model (Fig. 4A). As might be expected for such a large number of parameters, they were not uniquely constrained by the data. However, it was clear that synaptic transmission needed to have a high gain for single photons, meaning that the sum of ha and hb needed to be roughly six or more. This high gain produced a binary synapse that saturated during single photon transmission, effectively identical to the assumption of the binary Poisson model. Although the intensity–response relation could be fit with ha and hb = 1, this produced a multiphoton synapse with the result that for a given I_{max} and N_r the predicted variance was much too low. Thus, the intensity dependence of the variance-to-mean ratio suggests binary transmission at this synapse.

Our second goal was to investigate possible mechanisms of noise suppression at the RBC synapse. Direct evidence for noise suppression in the mouse retina is shown in Fig. 2A. The ratio I_{max}/i_s predicts an apparent convergence of 27 for this cell. Taking a S/N ratio for rod single photon events of 3–4 (Schneeweis & Schnapf, 2000; Field & Rieke, 2002), if the RBC summed linearly, the noise would increase by a factor of about 5 and even the two photon events should have remained buried in the noise. Alternatively, our results would imply a linear convergence of less than three rods to be consistent with the S/N ratio of 1.8 observed in this RBC. The S/N ratio was evaluated as σ/i_q in five cells and averaged 2.4 ± 0.6. Thus, the observation of single photon events requires a nonlinearity during transmission to account for the data.

The effects of noise for a linear model are shown in Figs. 4B–4C. During simulations, noise was added to the rod signals (dark continuous noise standard deviation. $\sigma_d = i_q * 0.27$, photon event amplitude standard deviation $\sigma_q = i_q * 0.33$) in line with the S/N ratio of single photon signals observed in mouse rods (Field & Rieke, 2002). The convergent noise dominated the response at low intensities producing a much larger mean current compared with

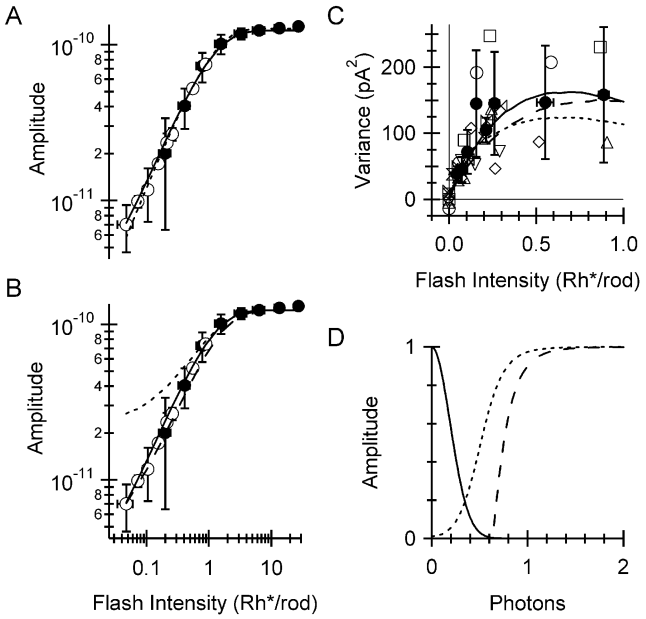

Fig. 4. Predictions from the Transmission model. A: Absolute amplitude of flash responses replotted from Fig. 1. The top panel shows a comparison of the Binary Poisson model (dotted line) and the noise-free Transmission model (solid line). The parameters were $B = 1.05$, $ha = 2$ and $hb = 4$, k_a, $k_b = 0.5$, with $i_q = 5.6$ pA and the $N_r = 22$. B: The noise-free Transmission model prediction from *A* (solid line) is compared with the prediction obtained with noise added ($\sigma_q = 0.33$, $\sigma_d = 0.27$, dotted line). The dashed line shows the effect of increasing *B* to 4 in the Transmission model. The other parameters were unchanged except that the rod collecting area, ϕ, had to be increased by 15% to compensate for the loss of low-amplitude events as illustrated in *D*. C: Corresponding predictions of the variance for the Transmission model with parameters as in *B*. D: RBC response as a function of the photon event amplitude in the noise-free case with $B = 1.05$ (dotted line), and the noise-suppressed condition with $B = 4$ (dashed line). The solid line shows the distribution of the baseline noise, with a standard deviation of $0.27 * i_q$ (Field & Rieke, 2002).

the noise-free model (Fig. 4B). Increasing *B* to 4 produced a sharp threshold in the RBC response (Fig. 4D), which effectively removed much of the noise and reestablished the agreement between model and data in Fig. 4B.

Discussion

Our results suggest that under dark-adapted conditions the gain at the first synapse can be high enough to saturate transmission when the connected rod captures one photon (Rao et al., 1994; Rao-Mirotznik et al., 1995; van Rossum & Smith, 1998). This means that RBCs can function as single photon detectors, and that each synaptic connection provides a binary signal—the occurrence, or not, of a photoisomerization within the connected rod. Our model envisages that signals are generated independently at each dendritic contact and then are summed linearly by the RBC. This model is supported by four observations. The mean amplitude of the average responses at low intensities is a linear function of the light intensity. There is very little change in the time course of RBC flash responses over much of the dynamic range, consistent with linear summation of the dendritic inputs. The variance saturates as expected for a binary synapse. There is excellent agreement between the rod-to-rod-bipolar convergence measured anatomically (Tsukamoto et al., 2001), and our physiological estimate predicted from the ratio of the saturating response to the single photon amplitude.

As noted above, single photon transmission implies the existence of a nonlinear mechanism that suppresses the convergent neural noise, and we explored such a mechanism first outlined by Shiells and Falk (1994). The postulated nonlinearity arises because the open probability of the mGluR6-operated channels cannot be less than zero. The biochemical gain (*B* in the model) ensures that all channels remain closed, even during moderate reductions in the mGluR6 receptor activation caused by voltage noise within the connected rod terminal. However, when the glutamate concentration falls to a low enough level the number of open channels is very steeply dependent on the change in concentration, due to the high cooperativity of receptor activation. Thus, the postsynaptic machinery acts as a nonlinear molecular switch, suppressing noise, but turning on suddenly when an event exceeds the threshold.

A recent study by Field and Rieke (2002) also examined transmission at the rod to RBC synapse in the mouse retina, and argued for a high threshold during synaptic transfer that resulted in the loss of 75% of the smaller single photon events. Since only the largest events were transmitted, the trial-to-trial variance at low mean response levels was larger than expected for a Poisson process. The present results differed. At low light levels the variance and mean increased as expected for a Poisson process, but at higher intensities the variance was lower than expected because the synapse saturated. A second notable difference was that Field and Rieke (2002) observed a supralinear increase in the amplitude of the response at intensities just below the half-saturating intensity. The present results were more linear. One possibility that would explain the differences is that the RBCs are working at different adaptation levels in the two studies. Field and Rieke (2002) recorded a half-saturating intensity of 2.8 Rh*/rod, about 4-fold higher than obtained in the present study (~0.7 Rh*/rod, using essentially the same rod collecting area). The half-saturating intensity estimated here is similar to that obtained for the PII component of the electroretinogram in mouse (Saszik et al., 2002). We argue below that the threshold should be higher in a more light-adapted situation.

Very large convergence of rod signals onto ganglion cells improves sensitivity (Copenhagen et al. 1990), but also accumulates their noise (Sterling et al., 1988; van Rossum & Smith, 1998), which necessitates a noise removal mechanism, envisaged as a nonlinear threshold. The rod's major noise sources, "continuous dark noise," due to the transduction mechanism, and "thermal events," due to spontaneous thermal isomerization of rhodopsin, have temporal characteristics identical to single photon events so they cannot be reduced by temporal filtering (Baylor et al., 1984; Rieke & Baylor, 1996). Both these noise sources will generate dark events when they exceed threshold in the absence of a photon, and therefore are indistinguishable from photon events in later visual stages. However, much of the continuous dark noise is low amplitude and can be greatly reduced by an amplitude threshold. Synaptic convergence increases the thermal isomerization rate from about 0.006 Rh*/s in each rod (Baylor et al., 1984) to about 5 Rh*/s in a ganglion cell (Sterling et al., 1988), or about one event per ganglion cell per rod integration time. This rate is close to the dark-event rate in ganglion cells (Barlow et al., 1971; Mastronarde, 1983), implying that the false positive rate due to the continuous dark noise cannot be much greater.

The modeling presented in Fig. 5 shows predictions appropriate for the *S*/*N* ratio of single photon events in mouse rods

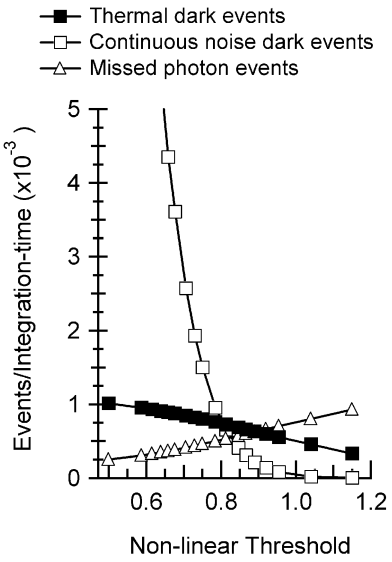

Fig. 5. Detection limits imposed by continuous dark noise and thermal events. Thermal dark events exceeded continuous noise dark events by a factor of 2 for thresholds greater than $0.85 * i_q$. For higher thresholds, the false positive rate drops precipitously and the false negative rate increases linearly. Simulations with the Transmission model were performed using different values of B to adjust the level of the nonlinear threshold, as a fraction of the single photon event amplitude. The output from the model was passed through a detection threshold, set to half the amplitude of the single photon event. Positive events (real and dark events) exceeded the threshold, while negative events did not. The standard deviation of the baseline noise in the rods (σ) was set to $0.27 * i_q$, and the standard deviation of the photon event amplitude (σ_q), was set to $0.33 * i_q$ (Field & Rieke, 2002). The light intensity, set to simulate the thermal isomerization rate in monkey, generated 0.00126 Rh*/rod/integration time (Baylor et al., 1984), using an integration time of 0.2 s for the single photon event in rods.

(Field & Rieke, 2002), and the thermal isomerization rate estimated in monkey rods (0.00126 Rh*/rod/rod integration time, Baylor et al., 1984). The false positive rate due to dark continuous noise is a strong function of the nonlinear threshold. For low thresholds (<0.8 single photon signal amplitudes), the false positive rate swamps the thermal event rate, with a correspondingly low false negative rate (<20%). Field and Rieke (2002) showed that although a synaptic threshold set at about 1.2 times the single photon response amplitude rejected 75% of the single photon signals, it obviated the effects of continuous noise in the rod array and increased the S/N ratio in the RBC by a factor of several hundred. As long as subsequent synaptic connections did not introduce additional noise, the ganglion cells could use the RBC output as a near optimal readout of the rod array. However, in starlight, most single photon events in the rod array result not from real photons, but from random thermal isomerizations, indistinguishable from real photon events and transmitted equally well. Although a threshold set at 1.2 times the single photon response amplitude would dramatically reduce the dark events due to dark continuous noise, it could not increase visual performance much because real photon events would still be masked by the much higher rate of thermal dark events. Further, such a high threshold would reduce detection of thermal and real photon events by ~2-fold, without affecting their ratio. Since later synaptic convergence stages add noise (Smith & Vardi, 1995; Hartveit, 1999; Freed, 2000; Singer & Diamond, 2003) such a reduction would be counter-productive because it would reduce the S/N ratio of the signal in ganglion cells or higher centers. In light of these considerations, we would argue that a lower threshold is more appropriate. Since the dark event rate, both continuous and thermal, limits ganglion cell sensitivity at visual threshold (Levick et al., 1983; Mastronarde, 1983), there would be little advantage in lowering the false positive rate much below the thermal rate. This implies that a nonlinear threshold around 0.85 would be appropriate, since the thermal event rate masks the false positives generated by continuous noise, while the false negative rate is a relatively modest 50% (Fig. 5).

As noted above, later stages of synaptic convergence add noise, which also requires a mechanism for its removal (Sterling et al., 1988; Smith & Vardi, 1995). We propose that each synaptic stage suppresses only that noise due the immediate convergence (20:1 for Rod → RBC, or 25:1 for RBC → AII), thus preserving the single photon S/N at each stage, and leaving the task of discriminating visual events from the thermal background to later synaptic stages, either at the ganglion cells or higher centers. This notion would be consistent with a lower threshold at the first synapse, and with the expectation that the statistics of photon capture by the RBCs should be closer to Poisson, as we have found. However, at higher background light levels with more incident photons, the threshold at the first synapse could be raised. The higher threshold would increase the fraction of missed photons resulting in a reduced sensitivity with a concomitant shift in the intensity–response relation. The higher threshold would also favor transmission of a multi-photon event in a rod, which is more likely to exceed the threshold than a single photon event. Such early coincidence detection would be a very effective mechanism to abrogate the background signal represented by thermal and uncorrelated visual events. In this high-threshold state, the statistics of photon capture by the system during very dim flashes would depart strongly from the Poisson expectation, contrary to our findings.

The scotopic rod pathway is known to adapt over a range of at least 3 log units (Sakmann et al., 1969; Sieving et al., 1986; Smith et al., 1986; Robson & Frishman, 1995), and it is conceivable that adaptation at the rod to RBC synapse might be achieved by adjustment of the nonlinear threshold (van Rossum & Smith, 1998). A possible mechanism is suggested by the properties of the type B horizontal cell axon terminals (HBAT) which exists in most mammals, and which contact several hundred to several thousand rods (Wässle et al., 1978; Peichl & Gonzalez-Soriano, 1994). If these horizontal cells are similar to others in providing negative feedback to photoreceptors, an increase in background would tend to depolarize rods, which would increase a rod's release of neurotransmitter, essentially producing a higher threshold for the single photon signal in the RBC (van Rossum & Smith, 1998). The slow kinetics and broad spatial extent of the HBAT would provide a continuous estimate of the time-averaged output from all rods across an area comparable in size to the receptive field of a ganglion cell. Moreover, it would adjust the threshold in response to any noise source, whether it is background light, thermal isomerizations, or continuous dark noise. Such a HBAT feedback mechanism would generate a nonlinear surround for the rod, because feedback of the surround to rods would be transmitted forward through the rod RBC synapse threshold. Consistent with this, ganglion cells at low scotopic backgrounds have a weak nonlinear "hidden" surround (Wiesel & Hubel, 1966; Enroth-Cugell & Lennie, 1975; Barlow & Levick, 1976; Kaplan et al., 1979).

The Transmission model suggests that vesicle release from rod terminals is almost completely suppressed during a single photon signal. However, a single photon hyperpolarizes a mammalian rod by about 1 mV, less than one-tenth of the full dynamic range (Schneeweis & Schnapf, 1995), suggesting that rod signals may be "clipped" during transmission to RBCs. Signal clipping has been documented during transmission from photoreceptors to horizontal cells in salamander, where only a small fraction of the dynamic range of the photoreceptors is transmitted to the postsynaptic cell (Attwell et al., 1987; Belgum & Copenhagen, 1988). How such clipping occurs is still unknown. In mammalian photoreceptors, at potentials close to the dark resting potential, voltage changes the open probability of calcium channels e-fold for every 6 mV at the steepest point (Taylor & Morgans, 1998). Even if glutamate release depended on the third or fourth power of the presynaptic Ca^{2+} concentration, it seems unlikely that the voltage-dependence of the calcium channels can account for the putative suppression of vesicle release during a photon event. However, the calcium channels were characterized in cone photoreceptors, and it is possible that the channels in rods are different (Morgans, 1999). Calcium channels have not been characterized in mammalian rods, and it is tempting to suggest that they might have greater voltage sensitivity.

Acknowledgments

We would like to thank Dr. Andrew James for advice and assistance with the mathematical formulation. This research was supported by grant MH48168 to R.G. Smith.

References

Ashmore, J.F. & Falk, G. (1980). The single-photon signal in rod bipolar cells of the dogfish retina. *Journal of Physiology (London)* **300**, 151–166.

Ashmore, J.F. & Falk, G. (1982). An analysis of voltage noise in rod bipolar cells of the dogfish retina. *Journal of Physiology (London)* **332**, 273–297.

Attwell, D., Borges, S., Wu, S.M. & Wilson, M. (1987). Signal clipping by the rod output synapse. *Nature* **328**, 522–524.

Barlow, H.B. & Levick, W.R. (1976). Threshold setting by the surround of cat retinal ganglion cells. *Journal of Physiology* **259**, 737–757.

Barlow, H.B., Levick, W.R. & Yoon, M. (1971). Responses to single quanta of light in retinal ganglion cells of the cat. *Vision Research Suppl* **3**, 87–101.

Baylor, D.A., Lamb, T.D. & Yau, K.W. (1979). Responses of retinal rods to single photons. *Journal of Physiology (London)* **288**, 613–634.

Baylor, D.A., Nunn, B.J. & Schnapf, J.L. (1984). The photocurrent, noise and spectral sensitivity of rods of the monkey Macaca fascicularis. *Journal of Physiology* **357**, 575–607.

Belgum, J.H. & Copenhagen, D.R. (1988). Synaptic transfer of rod signals to horizontal and bipolar cells in the retina of the toad (*Bufo marinus*). *Journal of Physiology* **396**, 225–245.

Berntson, A. & Taylor, W.R. (2000). Response characteristics and receptive field widths of on-bipolar cells in the mouse retina. *Journal of Physiology (London)* **524**, 879–889.

Calvert, P.D., Govardovskii, V.I., Krasnoperova, N., Anderson, R.E., Lem, J. & Makino, C.L. (2001). Membrane protein diffusion sets the speed of rod phototransduction. *Nature* **411**, 90–94.

Calvert, P.D., Krasnoperova, N.V., Lyubarsky, A.L., Isayama, T., Nicolo, M., Kosaras, B., Wong, G., Gannon, K.S., Margolskee, R.F., Sidman, R.L., Pugh, E.N., Jr., Makino, C.L. & Lem, J. (2000). Phototransduction in transgenic mice after targeted deletion of the rod transducin alpha-subunit. *Proceedings of the National Academy of Sciences of the U.S.A.* **97**, 13913–13918.

Chun, M.H., Han, S.H., Chung, J.W. & Wässle, H. (1993). Electron microscopic analysis of the rod pathway of the rat retina. *Journal of Comparative Neurology* **332**, 421–432.

Copenhagen, D.R., Hemila, S. & Reuter, T. (1990). Signal transmission through the dark-adapted retina of the toad (Bufo marinus). Gain, convergence, and signal/noise. *Journal of General Physiology* **95**, 717–732.

Dacheux, R. & Raviola, E. (1986). The rod pathway in the rabbit retina: A depolarizing bipolar and amacrine cell. *Journal of Neuroscience* **6**, 331–345.

Daw, N., Jensen, R. & Brunken, W. (1990). Rod pathways in mammalian retinae. *Trends in Neurosciences* **13**, 110–115.

Enroth-Cugell, C. & Lennie, P. (1975). The control of retinal ganglion cell discharge by receptive field surrounds. *Journal of Physiology* **247**, 551–578.

Famiglietti, E.V.J. & Kolb, H. (1975). A bistratified amacrine cell and synaptic circuitry in the inner plexiform layer of the retina. *Brain Research* **84**, 293–300.

Field, G.D. & Rieke, F. (2002). Nonlinear signal transfer from mouse rods to bipolar cells and implications for visual sensitivity. *Neuron* **34**, 773–785.

Freed, M.A. (2000). Rate of quantal excitation to a retinal ganglion cell evoked by sensory input. *Journal of Neurophysiology* **83**, 2956–2966.

Hartveit, E. (1999). Reciprocal synaptic interactions between rod bipolar cells and amacrine cells in the rat retina. *Journal of Neurophysiology* **81**, 2923–2936.

Hecht, S., Schlaer, S. & Pirenne, M. (1942). Energy, quanta and vision. *Journal of General Physiology* **25**, 819–840.

Hetling, J.R. & Pepperberg, D.R. (1999). Sensitivity and kinetics of mouse rod flash responses determined in vivo from paired-flash electroretinograms. *Journal of Physiology* **516** (Pt 2), 593–609.

Kaplan, E., Marcus, S. & So, Y.T. (1979). Effects of dark adaptation on spatial and temporal properties of receptive fields in cat lateral geniculate nucleus. *Journal of Physiology* **294**, 561–580.

Lamb, T.D. (1995). Photoreceptor spectral sensitivities: Common shape in the long-wavelength region. *Vision Research* **35**, 3083–3091.

Levick, W., Thibos, L., Cohn, T., Catanzaro, D. & Barlow, H. (1983). Performance of cat retinal ganglion cells at low light levels. *Journal of General Physiology* **82**, 405–426.

Mastronarde, D.N. (1983). Correlated firing of cat retinal ganglion cells. II. Responses of X- and Y-cells to single quantal events. *Journal of Neurophysiology* **49**, 325–349.

Morgans, C.W. (1999). Calcium channel heterogeneity among cone photoreceptors in the tree shrew retina. *European Journal of Neuroscience* **11**, 2989–2993.

Peichl, L. & Gonzalez-Soriano, J. (1994). Morphological types of horizontal cell in rodent retinae: A comparison of rat, mouse, gerbil, and guinea pig. *Visual Neuroscience* **11**, 501–517.

Penn, R. & Hagins, W. (1972). Kinetics of the photocurrent of retinal rods. *Biophysical Journal* **12**, 1073–1094.

Rao, R., Buchsbaum, G. & Sterling, P. (1994). Rate of quantal transmitter release at the mammalian rod synapse. *Biophysical Journal* **67**, 57–63.

Rao-Mirotznik, R., Harkins, A.B., Buchsbaum, G. & Sterling, P. (1995). Mammalian rod terminal: Architecture of a binary synapse. *Neuron* **14**, 561–569.

Rieke, F. & Baylor, D. (1996). Molecular origin of continuous dark noise in rod photoreceptors. *Biophysical Journal* **71**, 2553–2572.

Robson, J.G. & Frishman, L.J. (1995). Response linearity and kinetics of the cat retina: The bipolar cell component of the dark-adapted electroretinogram. *Visual Neuroscience* **12**, 837–850.

Sakitt, B. (1972). Counting every quantum. *Journal of Physiology* **223**, 131–150.

Sakmann, B., Creutzfeldt, O. & Scheich, H. (1969). An experimental comparison between the ganglion cell receptive field and the receptive field of the adaptation pool in the cat retina. *Pflugers Archive* **307**, 133–137.

Saszik, S.M., Robson, J.G. & Frishman, L.J. (2002). The scotopic threshold response of the dark-adapted electroretinogram of the mouse. *Journal of Physiology* **543**, 899–916.

Schneeweis, D. & Schnapf, J. (1995). Photovoltage of rods and cones in the macaque retina. *Science* **268**, 1053–1056.

Schneeweis, D.M. & Schnapf, J.L. (2000). Noise and light adaptation in rods of the macaque monkey. *Visual Neuroscience* **17**, 659–666.

Shiells, R.A. & Falk, G. (1994). Responses of rod bipolar cells isolated from dogfish retinal slices to concentration-jumps of glutamate. *Visual Neuroscience* **11**, 1175–1183.

Sieving, P.A., Frishman, L.J. & Steinberg, R.H. (1986). Scotopic threshold response of proximal retina in cat. *Journal of Neurophysiology* **56**, 1049–1061.

Singer, J.H. & Diamond, J.S. (2003). Sustained Ca^{2+} entry elicits transient postsynaptic currents at a retinal ribbon synapse. *Journal of Neuroscience* **23**, 10923–10933.

Smith, R. & Vardi, N. (1995). Simulation of the AII amacrine cell of mammalian retina: Functional consequences of electrical coupling and regenerative membrane properties. *Visual Neuroscience* **12**, 851–860.

Smith, R.G., Freed, M.A. & Sterling, P. (1986). Microcircuitry of the dark-adapted cat retina: Functional architecture of the rod-cone network. *Journal of Neuroscience* **6**, 3505–3517.

Sterling, P., Freed, M.A. & Smith, R.G. (1988). Architecture of rod and cone circuits to the on-beta ganglion cell. *Journal of Neuroscience* **8**, 623–642.

Strettoi, E., Dacheux, R. & Raviola, E. (1990). Synaptic connections of rod bipolar cells in the inner plexiform layer of the rabbit retina. *Journal of Comparative Neurology* **295**, 449–466.

Taylor, W.R. & Morgans, C.W. (1998). Localization and properties of voltage-gated calcium channels in cone photoreceptors of Tupaia belangeri. *Visual Neuroscience* **15**, 541–552.

Tsukamoto, Y., Morigiwa, K., Ueda, M. & Sterling, P. (2001). Microcircuits for night vision in mouse retina. *Journal of Neuroscience* **21**, 8616–8623.

van Rossum, M.C. & Smith, R.G. (1998). Noise removal at the rod synapse of mammalian retina. *Visual Neuroscience* **15**, 809–821.

Wässle, H., Boycott, B. & Peichl, L. (1978). Receptor contacts of horizontal cells in the retina of the domestic cat. *Proceedings of the Royal Society B (London)* **203**, 247–267.

Wässle, H., Yamashita, M., Greferath, U., Grünert, U. & Müller, F. (1991). The rod bipolar cell of the mammalian retina. *Visual Neuroscience* **7**, 99–112.

Wiesel, T.N. & Hubel, D.H. (1966). Spatial and chromatic interactions in the lateral geniculate body of the rhesus monkey. *Journal of Neurophysiology* **29**, 1115–1156.

Wyszecki, G. & Stiles, W. (1967). Colour Science. New York: John Wiley & Sons, Inc.